

Self-regulation of the reconnecting current layer in relativistic pair plasma reconnection

S. Zenitani and M. Hesse

NASA Goddard Space Flight Center, Greenbelt, MD 20771, USA

ABSTRACT

We investigate properties of the reconnecting current layer in relativistic pair plasma reconnection. We found that the current layer self-regulates its thickness when the current layer runs out current carriers and so relativistic reconnection retains a fast reconnection rate. Constructing a steady state Sweet-Parker model, we discuss conditions for the current sheet expansion. Based on the energy argument we conclude that the incompressible assumption is invalid in relativistic Sweet-Parker reconnection. The guide field cases are more incompressible than the anti-parallel cases, and we find a more significant current sheet expansion.

Subject headings: magnetic fields — plasmas — relativity

1. INTRODUCTION

Magnetic reconnection (Vasyliunas 1975; Biskamp 2000; Birn & Priest 2007) is the driver of explosive events in space plasmas and laboratory experiments. Although it has extensively been studied over since 1950s, its detailed mechanism still remains unclear. The complexity of the reconnection problem is that small-scale physics in and around the reconnecting X -type region (or the diffusion region) can drastically change the system's global evolution.

Magnetic reconnection has drawn attention in various high-energy astrophysical applications (Coroniti 1990; Drenkhahn & Spruit 2002; Lyutikov 2003), where a relativistic extension of magnetic reconnection in an electron positron pair plasma (e^\pm) is considered. However, the physical mechanism of relativistic magnetic reconnection, as well that of the well-studied non-relativistic reconnection, is far from being understood. For example, only a few researchers have developed fundamental models of relativistic steady-state reconnection. Blackman & Field (1994) predicted that relativistic magnetic reconnection facilitates faster energy conversion than non-relativistic reconnection, due to the Lorentz contraction in the outflow region. Lyutikov & Uzdensky (2003) followed them, but Lyubarsky (2005) claimed

that reconnection inflow can not be so fast. He further worked on the generalization of relativistic Petschek reconnection, and argued that the guide field (out-of-plane field) opposes energy conversion into the plasma energy.

On the other hand, self-consistent simulations have revealed important aspects of relativistic magnetic reconnection. Several authors (Zenitani & Hoshino 2001, 2005b, 2007, 2008; Jaroschek et al. 2004; Bessho & Bhattacharjee 2007) carried out particle-in-cell (PIC) simulations of relativistic pair plasma reconnection, and they found that powerful particle acceleration occurs inside/near the diffusion region. The main accelerator is the reconnection electric field, which becomes strong enough to sustain relativistic outflow. When the system contains a guide field, relativistic magnetic reconnection also involves particle acceleration by the reconnection electric field (Zenitani & Hoshino 2005b, 2008; Karlický 2008). It seems that particle acceleration by the reconnection electric field is a common feature of relativistic magnetic reconnection. Furthermore, carrying out a relativistic magnetohydrodynamic (RMHD) simulation, Watanabe & Yokoyama (2006) presented a Petschek structure in mildly-relativistic regime. Note that they assume spatially limited resistivity, representing the physics inside the diffusion region.

In an ion-electron plasma, it is known that a thin current layer appears near the X point during magnetic reconnection (Horiuchi & Sato 1994). The main current carriers are electrons, and the thin electron current layer is a key region to understand the reconnection physics. So, significant efforts have been paid to the evolution of the electron diffusion region (Hesse & Winske 1998; Hesse et al. 1999). The general consequence will be that the current layer becomes thin as reconnection develops, typically into the electron meandering width (Horiuchi & Sato 1994). On the other hand, there is an ongoing discussion on the length of the current layer (Fujimoto 2006; Daughton et al. 2006; Shay et al. 2007), whose extension may regulate the reconnection rate by changing the aspect ratio of the “diffusion” region.

In a relativistic pair plasma, few attention has paid to the detail structure of the diffusion region, although it is a key region to drive magnetic reconnection and to accelerate high-energy particles. Recently, Hesse & Zenitani (2007) investigated the composition of the reconnection electric field and they showed that the off-diagonal parts of the pressure tensor are important, similarly to the non-relativistic cases (Hesse et al. 1999, 2004; Bessho & Bhattacharjee 2007). However, a physical interpretation of the off-diagonal terms has not yet well-established, as well as the terms in a true decomposition of the relativistic pressure tensor. In the present paper, we investigate the properties of the diffusion region in relativistic pair plasma reconnection from another viewpoint: the temporal development of the reconnecting current layer. The unexpected new result is that the out-of-plane current layer adjusts itself by expanding its thickness. When the plasma drift velocity reaches to

an upper limit, typically on an order of the light speed, the current layer runs out current carriers. Then, the reconnection electric field becomes stronger to satisfy the Ampère’s Law for the field reversal current. Consequently, the non-MHD diffusion region and the current layer becomes wider. Since it enhances the reconnection electric field and since it improves the aspect ratio of the dissipation region, relativistic reconnection retains a fast reconnection rate. A brief discussion of the steady-state energy flow provides some insight into this process. We cannot employ the incompressible assumption in relativistic Sweet-Parker condition any more. The guide field brings incompressibility, and therefore we find a more significant current sheet expansion.

The paper consists of the following sections. In §2 we describe our simulation setup and briefly overview the system evolution. In §3 we extended our interpretation by using a steady-state Sweet-Parker model. In §4 we discuss the guide field extension. Finally, §5 contains discussion and the summary.

2. SIMULATION & RESULTS

We carry out two-dimensional PIC simulations in the x - z plane. As an initial current sheet configuration, we employ a relativistic extension of the Harris model. The magnetic field, plasma density and plasma distribution functions are described by $\mathbf{B} = B_0 \tanh(z/L)\hat{\mathbf{x}} + B_G\hat{\mathbf{y}}$, $d(z) = (\gamma_\beta n_0) \cosh^{-2}(z/L)$ and $f_s \propto d(z) \exp[-\gamma_\beta\{\varepsilon - \beta_s u_y\}/T]$. In the above equations, B_0 is the magnitude of antiparallel magnetic field, B_G is the out-of-plane magnetic field, L is the typical thickness of the current sheet, n_0 is the proper number density of plasmas in the current sheet, the subscript s denotes the species (p for positrons, e for electrons), $\beta_p = -\beta_e = \beta$ is the dimensionless drift velocity, γ_β is the Lorentz factor for β ($\gamma_\beta = [1 - \beta^2]^{-1/2}$), ε is the particle energy, \mathbf{u} is the relativistic four velocity of $\mathbf{u} = [1 - (v/c)^2]^{-1/2}\mathbf{v}$ and T is the proper temperature including the Boltzmann constant. We set $T = mc^2$ and $\beta = 0.3$, respectively. In addition, a uniform background plasma is added to the system. Its number density and temperature are $n_{bg}/(\gamma_\beta n_0) = 5\%$ and $T_{bg}/mc^2 = 0.1$, respectively. This background temperature is cold enough that the background plasma energy density is $\sim 1.2n_{bg}mc^2$ per species, including the rest mass energy. The plasma satisfies the pressure balance condition $B_0^2/8\pi = 2n_0T$ in this equilibrium. The Debye length is $[T/(4\pi\gamma_\beta^2 n_0 q^2)]^{1/2} = 0.3L$, where q is the charge. The typical Larmor radius is $c(qB_0/\gamma mc)^{-1} \sim 0.2L$.

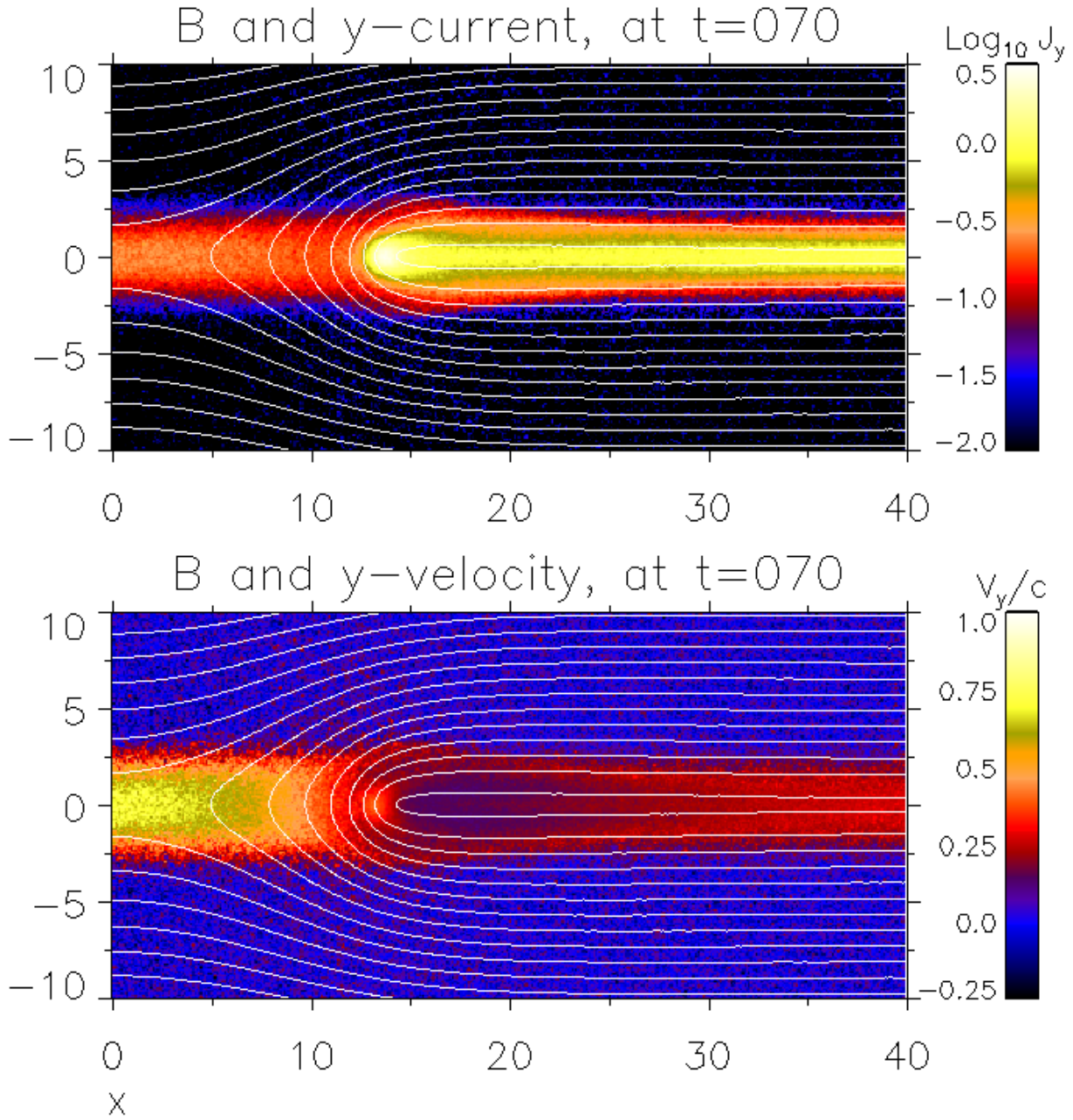
The system consists of $1536(x) \times 768(z)$ cells and the typical scale of the current sheet L is set to 10 cells. We consider periodic boundaries in the x direction, and the boundaries are located in $x = \pm 76.8L$. We also consider periodic boundaries in the z direction, but

we divide the simulation domain into two sub domains. The first half (the main simulation domain) is located in $-19.2L \leq z \leq 19.2L$, and the other half (the sub simulation domain) is located in $19.2L \leq z \leq 57.6L$. In the sub domain, we assume an oppositely directed Harris model (e.g. $\mathbf{B} = -B_0 \tanh[z/L - 38.4]\mathbf{x}$), so that physical properties in the sub domain are smoothly connected to those in the main domain. We use 7.6×10^7 super particles in this simulation. One cell contains 6.4×10^2 particles at the center of the current sheet. The detailed parameters are presented in Table 1. During the very early stage of the simulation, we set small driving force to trigger magnetic reconnection near the center of the simulation domain. This trigger field smoothly varies in time, and it is applied until $t \sim 12\tau_c$, where $\tau_c = L/c$ is the light transit time, while we discuss the physics of reconnection in the late stage of $30\tau_c \sim 90\tau_c$. The total energy is conserved within an error of 0.1% throughout the simulation run, after the initial trigger force vanishes. In addition, we carry out four runs with different parameters of $n_{bg}/(\gamma_\beta n_0)$ and B_G/B_0 . Their parameters are shown in Table 1. These configurations are similar to previous simulations (Zenitani & Hoshino 2007, 2008).

Hereafter we describe the evolution of the first run (run 1). After the initial impact disappears, magnetic field lines start to reconnect around the center of the main simulation domain. The panels of Figure 1 present the snapshots of the reconnecting region at $t/\tau_c = 70$. The X -point is located at the left border ($x = 0$), while the simulation domain ranges $-76.8 < x/\lambda < 76.8$. The upper panel shows magnetic field lines and the y -current (out-of-plane component of the current) density. The lower panel shows magnetic field lines and the y component of the plasma average velocity. Notice that the X point is located around $x \sim 0$. At this stage, magnetic reconnection is well developed: the plasma outflow velocity ($\langle v_x \rangle$) is up to $\sim 0.7c$ around outflow region.

Panels in Figure 2 present the plasma number density $2n$, the current density J_y , average drift velocity $\langle v_y \rangle$, and reconnection electric field E_y along the inflow line $x = 0$. These values are averaged over $-1/4 \leq x/L \leq 1/4$ in order to reduce noise. The y -current is carried by the drift motion of positrons ($+y$ direction) and electrons ($-y$ direction) inside the current sheet: $J_y \sim 2d(z)\langle v_y \rangle$. We present three characteristic stages at $t/\tau_c = 30, 50$ and 70 . Shortly before $t/\tau_c = 30$, reconnection is about to begin: $\langle v_y \rangle$ and E_y start to increase around the X -type region, while plasma density start to decrease there because plasmas flow away into the reconnection outflow region. At $t/\tau_c = 50$, the reconnecting current layer looks “thin” around the reconnecting region, and then the plasma inflow and outflow structures are developed. The $\langle v_y \rangle$ goes up to $\sim 0.7c$ around the center.

After $t/\tau_c = 50$, the current layer shows an unexpected evolution which is not explained by present reconnection theories. Previous studies show current layers, which are substantially thinner than the initial current sheet. However, in this case, the current sheet starts to



▣

Fig. 1.— Magnetic field lines and y component of (a) the current density and (b) the average velocity at $t/\tau_c = 70$ in run 1. }

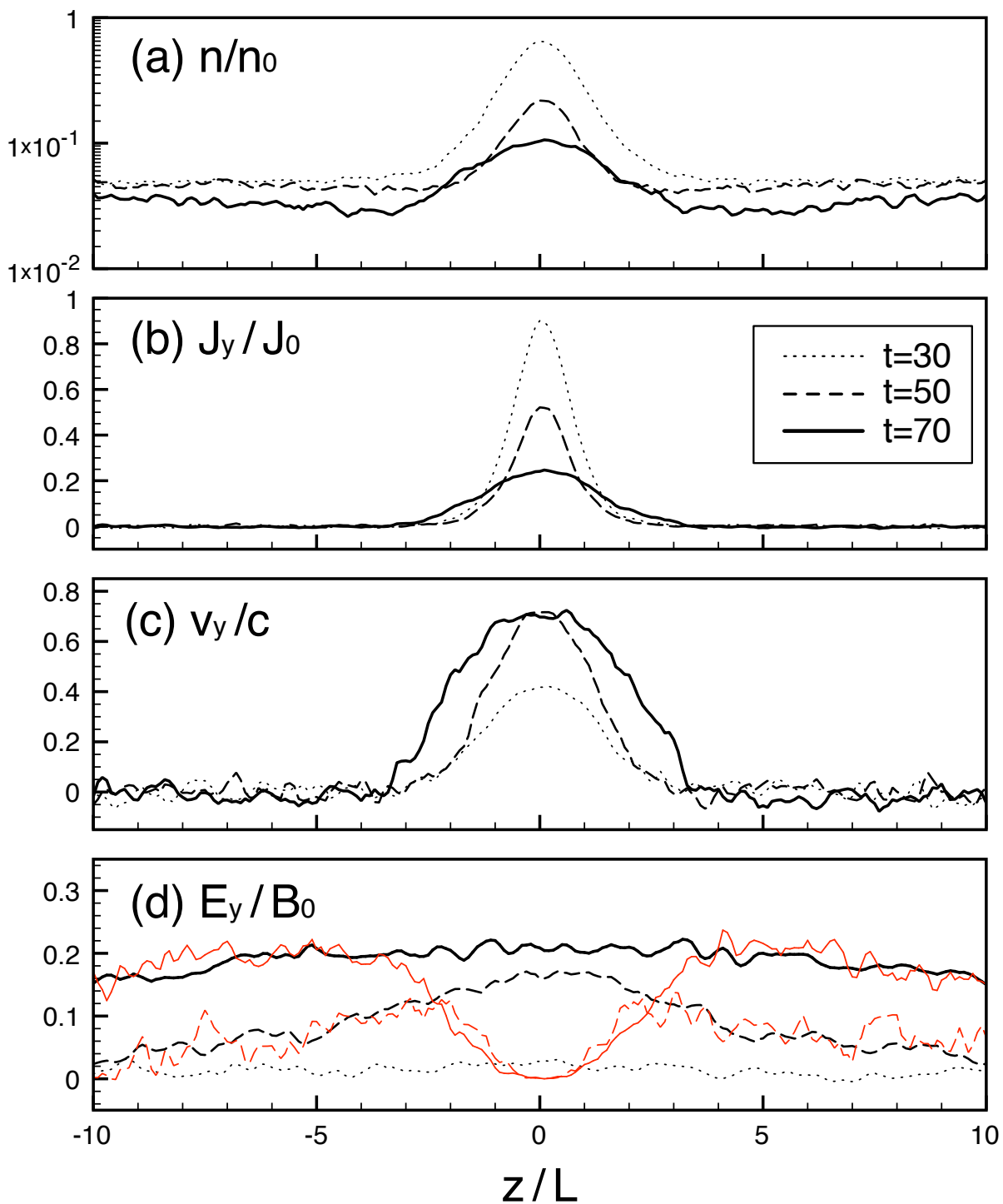


Fig. 2.— Physical properties along the inflow region at $x/L = 0$ in run 1: (a) Normalized plasma density, (b) y -component of the electric current, (c) y -component of the plasma average velocity, and (d) Reconnection electric field E_y . The red lines show the relevant $(-\mathbf{v} \times \mathbf{B})_y$ electric fields.

expand. The change may look small in Figure 1, but we can clearly recognize the expansion signature in Figures 2*b* and 2*c*. The plasma velocity $\langle v_y \rangle$ and the current density J_y increase outside the initial current sheet. In fact, J_y outside the current sheet is more stronger than the initial state, which was almost zero. Figure 3*a* (*black line*) presents the time evolution of the current sheet thickness measured by the scale height or the relative amplitude of the current density $|J_y|$. During the preflight stage, the current sheet becomes slightly thinner than the initial Harris sheet thickness, but it starts to expand, and finally it becomes ~ 1.9 times wider after $t/\tau_c = 70$.

Figure 3*b* shows time evolution of the reconnection rate, represented by the electric field E_y at the X -point. In this two-dimensional configuration, the reconnection rate E_y/B_0 immediately indicates the efficiency of magnetic energy conversion. The rate is often normalized by the reconnection outflow speed in non-relativistic study, but we normalize the rate by c since the outflow is on an order of $\sim 0.7c$. So, although this rate may be slightly underestimated, we obtain a relatively fast reconnection rate of 0.15-0.2. This rate is faster than the well-known non-relativistic reconnection rates of ~ 0.1 , due to the E_y -enhancement along with the current sheet expansion.

Next, let us interpret the physics of the current sheet expansion. In this simulation, we use a large density ratio of Harris sheet plasmas to the background plasmas: $n_{bg}/(\gamma_\beta n_0) = 5\%$. Once reconnection starts, dense Harris sheet plasmas escape into the outflow region, while only less dense background plasma enters the reconnecting region. Therefore, the plasma density continues to decrease as seen in Figure 2*a*. The density finally decreases to about the background density. Consequently, the system starts to run out the y -current J_y for the field reversal around the diffusion region. Recall the restriction of the Ampère’s Law: the system needs the out-of-plane current J_y .

$$(\nabla \times \mathbf{B})_y = \frac{4\pi}{c} J_y + \frac{1}{c} \frac{\partial E_y}{\partial t} \quad (1)$$

However, the system needs to maintain the field reversal.

The first workaround is to enhance the plasma current $J_y = 2d_{cs}\langle v_y \rangle$, where d_{cs} is the number density in the current sheet. In non-relativistic regime, the plasma current J_y is simply enhanced by particle acceleration into the $\pm y$ -directions. The displacement current works indirectly, because the enhanced electric field E_y accelerates particles. In fact, at $t/\tau_c \lesssim 50$, the reconnection electric field E_y and the plasma y -velocity $\langle v_y \rangle$ are significant only around the center ($z \sim 0$) (Figs. 2*c* and 2*d*). However, in a relativistic plasma, the plasma current has an upper limit of $|\mathbf{J}| < 2d_{cs}c$. When the velocity becomes an order of c , plasmas can not carry any more currents.

The next workaround is to directly use the displacement current $(1/c)(\partial \mathbf{E}/\partial t)$. Indeed,

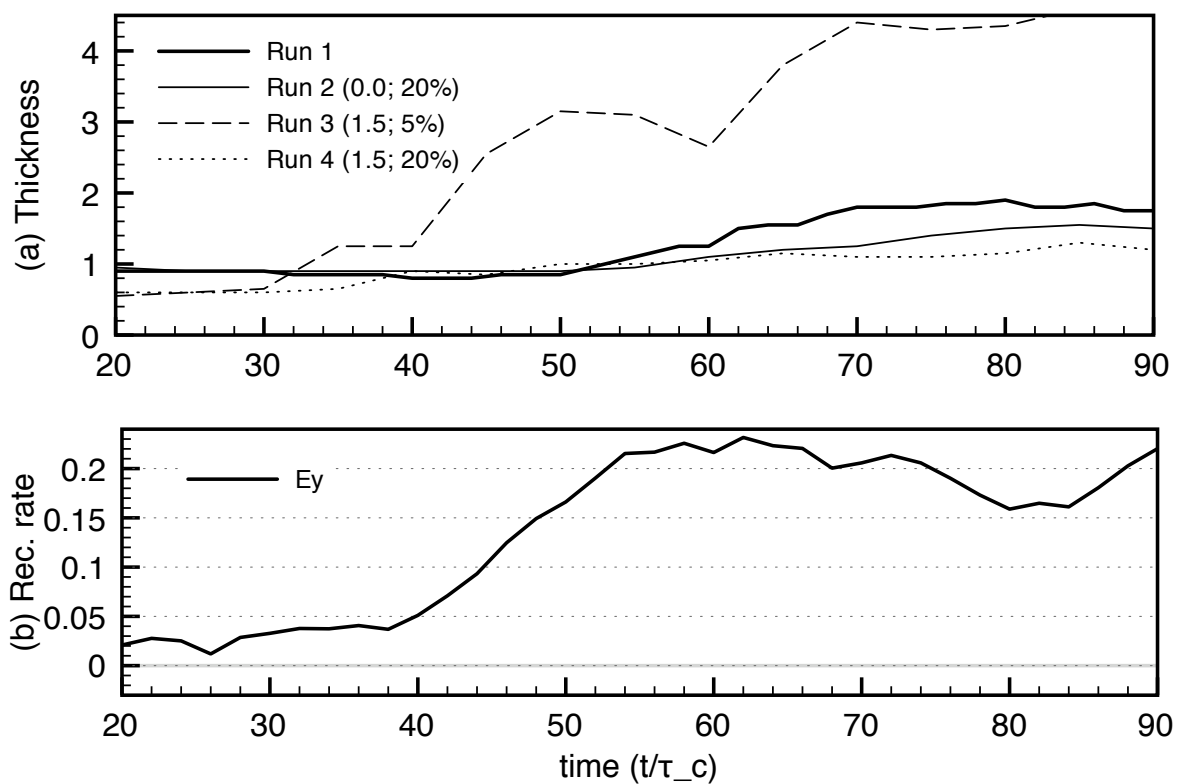


Fig. 3.— (a) Temporal evolution of the current sheet thickness at $x/L = 0$, measured by the scale height of the current density ($\log J_y$). (b) Temporal evolution of the reconnection rate (E_y/B_0) in run 1.

in this case, the plasma current explains only 80% of the required current and the displacement current accounts for the rest 20% around the turning phase of $t/\tau_c \sim 50$. However, the system can not use the displacement current to maintain a steady or quasi-steady structure. This workaround is temporal, and then the system goes into the other phase around $t/\tau_c \sim 50$.

Due to the effects of the displacement current term, the current layer starts to expand by the derivative of the generated electric field. Due to the displacement current, the electric fields E_y becomes even stronger across the current layer. This reduces magnetic fields outside the current layer.

$$\frac{\partial B_x}{\partial t} = -(c\nabla \times \mathbf{E})_x \sim c \frac{\partial E_y}{\partial z}. \quad (2)$$

Note that $B_x > 0$ and $(\partial E_y/\partial z) < 0$ on the upper side ($z > 0$), while $B_x < 0$ and $(\partial E_y/\partial z) > 0$ on the lower side ($z < 0$). Consequently, the MHD frozen-in condition breaks down over the wider spatial region around the neutral sheet. The red lines in Figure 2d present $(-\mathbf{v} \times \mathbf{B})_y$ at the relevant stages. We recognize that the non-MHD diffusion region of $E_y \neq (-\mathbf{v} \times \mathbf{B})_y$ becomes wider during $t/\tau_c = 50 \rightarrow 70$. Obviously the non-MHD region corresponds to the plasma drift region of $\langle v_y \rangle \gtrsim 0$. Since plasmas are free from the frozen-in restriction within the diffusion region, they are accelerated into the $\pm y$ directions by the enhanced electric field E_y , and then they start to carry the y -current. At $t/\tau_c = 70$ we can recognize that the outer regions around $z/L \sim \pm 2$ carry the y -current (Figs. 2b and 2c) and become a part of the diffusion region (Fig. 2d). The enlarged diffusion region involves more plasmas outside the initial current sheet, and then they are responsible for the required J_y for the field reversal.

In Fig. 2, we can compare the trend of the current sheet thickness and the reconnection electric field. The reconnection electric rate E_y increases first and then it stops before $t/\tau_c \sim 60$. The current sheet thickness slightly delays to the reconnection electric field, and it starts to expand. The current sheet remains nearly constant after $t/\tau_c = 70$ -80.

3. ANALYTIC THEORY

In order to understand the current sheet expansion, we consider a steady state Sweet-Parker current sheet model as presented in Figure 4. This model is too simple to discuss the detail properties of simulation runs, but sufficient to understand the physics. In addition, as long as we consider mildly relativistic regime of our scope, the current layer has a simple planar structure around the entire reconnecting region (Fig. 1). In Figure 4 the subscripts *in* and *out* denote the physical properties in the inflow region and in the outflow region, respectively. The current sheet width and height are $2L_{in}$ and $2L_{out}$. In the steady state,

conservation of magnetic flux, the number density continuity and energy budget in the model current sheet are written as

$$B_{in}v_{in} = B_{out}v_{out} \quad (3)$$

$$\gamma_{in}n_{in}L_{in}v_{in} = \gamma_{out}n_{out}L_{out}v_{out} \quad (4)$$

$$\left(2\gamma_{in}^2w_{in} + \frac{B_{in}^2}{4\pi}\right)L_{in}v_{in} = \left(2\gamma_{out}^2w_{out} + \frac{B_{out}^2}{4\pi}\right)L_{out}v_{out}, \quad (5)$$

where $w = e + p$ is the plasma enthalpy density: the sum of the plasma internal energy (e) and the proper pressure (p). We introduce the factor of 2 in eq. 5 so that we consider both electrons and positrons. In the x - z plane, we can assume that two species move together. By using the ratio of Poynting flux to the particle energy flux:

$$\sigma = \frac{B^2}{4\pi(2\gamma^2w)}, \quad (6)$$

eq. 5 can also be written as

$$\left(\frac{1 + \sigma_{in}}{\sigma_{in}}\right)\frac{B_{in}^2}{4\pi}L_{in}v_{in} = \left(2\gamma_{out}^2w_{out} + \frac{B_{out}^2}{4\pi}\right)L_{out}v_{out}. \quad (7)$$

Note that the relativistic Alfvén velocity is $V_A = \sqrt{\sigma/[1 + \sigma]}$ and the relevant Lorentz factor is $\gamma_A = \sqrt{1 + \sigma}$. In a cold plasma limit, σ_{in} is roughly reciprocal to the background plasma density ($n_{bg}/\gamma_\beta n_0$). Considering the initial equilibrium condition $B_0^2/8\pi = 2n_0T$ and the inflow plasma number density $\gamma_{in}n_{in} \sim n_{bg}$, some algebra yields

$$\sigma_{in} \sim \frac{2n_0T}{\gamma_{in}^2 n_{in} mc^2} \sim \frac{2}{\gamma_\beta \gamma_{in}} \frac{\gamma_\beta n_0}{n_{bg}} \frac{T}{mc^2} \quad (8)$$

In the case of non-relativistic antiparallel reconnection, in the limit of $(v_{in}/v_{out}) = \nu \ll 1$ these conditions lead to

$$d_{in}L_{in}v_{in} = d_{out}L_{out}v_{out} \quad (9)$$

$$\left(\frac{B_{in}^2}{4\pi}\right)L_{in}v_{in} \sim \left(2d_{out}\frac{mv_{out}^2}{2}\right)L_{out}v_{out}. \quad (10)$$

Note that we use the simulation frame density $d = \gamma n$ here. We obtain a familiar estimate of

$$v_{out} \sim \sqrt{\frac{B_{in}^2}{4\pi md_{in}}} = \sqrt{2} V_{Ain}. \quad (11)$$

Notice that the Alfvén speed in an electron positron plasma is $V_A = B/[4\pi(2md)]^{1/2}$ in the non-relativistic limit.

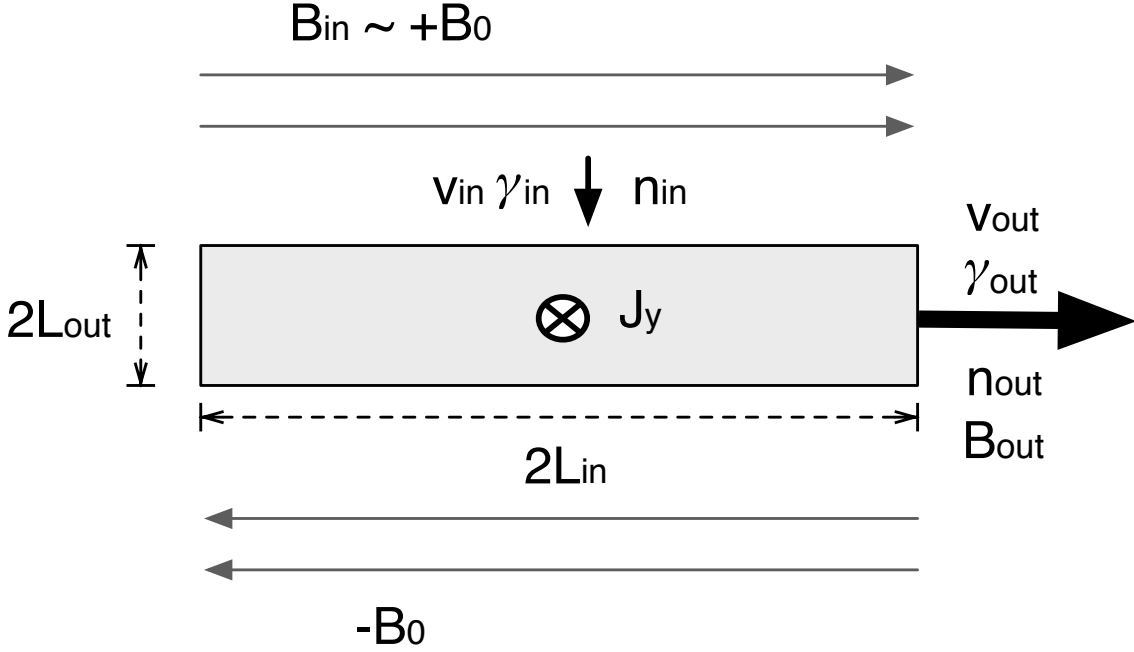


Fig. 4.— Simple model for a Sweet-Parker current sheet. Inflow properties and outflow properties are represented by subscripts *in* and *out*, respectively.

Let's consider the relativistic case. For simplicity, we assume that incoming flow is flux-dominated: the magnetic energy carries most of the incoming energy. So, we drop w_{in} from the left hand side of eq. 5. This approximation is appropriate for our low-background density runs, because we set a low density background plasmas ($n_{bg}/[\gamma_{\beta}n_0] \ll 1$) in a nonrelativistic temperature ($T_{bg} \ll mc^2$). In addition, we approximate the enthalpy term in the relativistic pressure limit

$$w_{out} = (e_{out} + p_{out}) \sim \left(n_{out}mc^2 + \frac{\Gamma p_{out}}{\Gamma - 1} \right) \sim 4p_{out} \quad (12)$$

where $\Gamma \sim 4/3$ is the adiabatic index. In the outflow region, the pressure balance across the current sheet (Lyubarsky 2005) yields

$$\frac{B_{in}^2}{8\pi} = 2p_{out} \quad (13)$$

Using eqs. 7 and 13 and introducing $\nu = v_{in}/v_{out}$, we obtain

$$\left(\frac{1 + \sigma_{in}}{\sigma_{in}} \right) 4p_{out} L_{in} v_{in} \sim (8\gamma_{out}^2 + 4\nu^2) p_{out} L_{out} v_{out} \quad (14)$$

The number density yields

$$\frac{\gamma_{out} n_{out}}{\gamma_{in} n_{in}} = \frac{L_{in} v_{in}}{L_{out} v_{out}} \sim \left(\frac{\sigma_{in}}{1 + \sigma_{in}} \right) (2\gamma_{out}^2 + \nu^2) \quad (15)$$

In the limit of $\nu^2 \ll 1$ and $\sigma_{in} \gg 1$, we obtain

$$\frac{\gamma_{out} n_{out}}{\gamma_{in} n_{in}} \sim 2\gamma_{out}^2 \quad (16)$$

in simulation frame density, or $(n_{out}/n_{in}) \sim 2\gamma_{in}\gamma_{out}$ in proper density. This analysis tells us that the relativistic steady-state reconnection is not incompressible both in the simulation frame and the proper frames. Previous reconnection models (Blackman & Field 1994; Lyutikov 2003) employ an incompressible assumption in the proper frames. Our analysis shows that the relativistic reconnection model should be re-constructed by taking compressibility into account. Incompressible models are helpful when and only when $\gamma_{out} \sim 1$.

We can confirm the above argument by using Lyubarsky (2005)'s analysis. For two fluids, the x -momentum conservation along the outflow line yields

$$2 \frac{\partial}{\partial x} \left(\frac{\gamma_{out}^2 w_{out} v_{out}^2}{c^2} + p_{out} \right) \sim \frac{1}{c} J_y B_{out} \quad (17)$$

Substituting $(\partial/\partial x) \sim 1/L_{in}$, $J_y \sim cB_{in}/(4\pi L_{out})$ and using eq. 12, we obtain

$$\left(\frac{4\gamma_{out}^2 v_{out}^2}{c^2} + 1 \right) p_{out} \sim \frac{L_{in}}{2} \frac{B_{in}}{4\pi L_{out}} B_{out} \quad (18)$$

Combining eqs. 4, 13 and 18, we obtain

$$\frac{\gamma_{out} n_{out}}{\gamma_{in} n_{in}} = \frac{L_{in} v_{in}}{L_{out} v_{out}} \sim \frac{4\gamma_{out}^2 (v_{out}/c)^2 + 1}{2} \sim 2\gamma_{out}^2 \quad (19)$$

Next, let's consider the current sheet thickness. In the steady state, the current in the central current sheet satisfies

$$\frac{cB_{in}}{4\pi L_{out}} = 2qd_{cs}v_y, \quad (20)$$

where d_{cs} is the typical number density in the current sheet. Also, the initial Harris condition satisfies

$$\frac{cB_0}{4\pi L} \sim \frac{cB_{in}}{4\pi L} = 2q(\gamma_{\beta} n_0)\beta c. \quad (21)$$

The ratio of the current sheet thickness yields

$$\frac{L_{out}}{L} = \frac{(\gamma_{\beta} n_0)\beta c}{d_{cs}v_y}. \quad (22)$$

We can evaluate the right hand side by considering the inflow number density $n_{bg} \sim \gamma_{in} n_{in}$, a central current sheet density $\gamma_{in} n_{in} \leq d_{cs} \leq \gamma_{out} n_{out}$, and the compressible factor of eq. 16:

$$\frac{(\gamma_{\beta} n_0)}{n_{bg}} \frac{(\gamma_{in} n_{in})\beta c}{d_{cs}v_y} \gtrsim \frac{(\gamma_{\beta} n_0)}{n_{bg}} \frac{\gamma_{in} n_{in}}{\gamma_{out} n_{out}} \frac{\beta c}{v_y} \sim \frac{(\gamma_{\beta} n_0)}{n_{bg}} \frac{1}{2\gamma_{out}^2} \frac{\beta c}{v_y}. \quad (23)$$

Then, eq. 22 rewrites

$$\frac{L_{out}}{L} \gtrsim \frac{(\gamma_\beta n_0)}{n_{bg}} \frac{\beta}{2\gamma_{out}^2} \left(\frac{c}{v_y}\right). \quad (24)$$

We recognize that the following condition is sufficient for the current sheet expansion

$$D = \frac{\gamma_\beta n_0}{n_{bg}} \frac{\beta}{2\gamma_{out}^2} \gtrsim 1, \quad (25)$$

where D is a discriminant term. Note that D also indicates the minimum relative thickness of the steady-state current sheet: $L_{out} \gtrsim DL$.

Since we do not have a perfect theory on the outflow gamma γ_{out} , we refer to the simulation results. In the case of run 1 ($t/\tau_c = 70$), the plasma x -velocity v_{out} and the electromagnetic field does not satisfy the frozen condition inside $x \lesssim 10L$, and so we regard the region as the diffusion region. Inside the diffusion region, the Lorentz factor of the averaged-flow $\gamma^2 = [1 - (\langle v_x \rangle^2 + \langle v_y \rangle^2)/c^2]^{-1} \sim 2$ stays constant in the diffusion region. The density stays small $d_{cs} \gtrsim 2n_{bg}$ and it gradually goes up in the outflow direction. Taking the results into account (e.g. $2\gamma_{out}^2 \sim 4$), we find that the condition (eq. 25) is already satisfied: $D = 1.5 > 1$. The observed thickness $\sim 1.9L$ is larger than $1.5L$. For comparison, we carried out the other run with dense background plasmas (run 2; $n_{bg}/\gamma_\beta n_0 = 20\%$), too. In this case, the current sheet expansion is less significant (*thin line* in Fig. 3a). Although the observed thickness $\sim 1.5L$ is rather larger than $D \sim 0.6$ primary due to the slow y -velocity of $\langle v_y \rangle \sim 0.5c$, it is reasonable that the current sheet expansion is less significant, because the inflow delivers more current carriers than in run 1.

4. GUIDE FIELD CASE

We also study the current sheet problem in the guide field case. Snapshots of run 3 with strong guide field $B_G/B_0 = 1.5$ are presented in Fig. 5. They are at the well-developed stage of $t/\tau_c = 140$. Note that the guide field reconnection evolves slower than the anti-parallel reconnection. The typical outflow speed is $v_{out} \sim 0.3c$. The structure of the reconnection region looks more complicated than the anti-parallel case. For example, we can see inclined current layers along the separatrix (Fig. 5a). There are also in-plane electric fields (E_x, E_z) due to the charge separation of positrons and electrons (Karlický 2008; Zenitani & Hoshino 2008). However, in order to discuss a zeroth-order structure of the diffusion region, similar Sweet-Parker approximation would be plausible. In fact, the y -velocity structure, which is a good indicator of the diffusion region structure, looks like rectangular structure (Fig. 5b). Panels in Figure 6 present the plasma properties along the inflow line $x = 0$, similar to those

of Fig. 2. Surprisingly, the plasma number density in the current sheet is slightly lower or almost same as the inflow density at the well-developed stage ($t/\tau_c = 140$; Fig. 6a). Plasma seems to be incompressible unlike the anti-parallel case. Plasma average y -velocity is even faster: $\langle v_y \rangle \sim 0.9c$ at $t/\tau_c = 80$ and $\langle v_y \rangle \sim 0.97c$ at $t/\tau_c = 140$ at the center. This is probably because the guide field confines particle motion into the y direction. Importantly, the current sheet looks much thicker than the anti-parallel case (Figs. 5a, 6b and c).

Next, let us consider a similar Sweet-Parker model. We set the guide field in the inflow region to B_{Gin} . The energy flux and pressure balance condition are modified in the following way

$$\left(\frac{B_{in}^2 + B_{Gin}^2}{4\pi}\right)L_{in}v_{in} = \left(2\gamma_{out}^2 w_{out} + \frac{B_{out}^2 + B_{Gout}^2}{4\pi}\right)L_{out}v_{out} \quad (26)$$

$$\frac{B_{in}^2 + B_{Gin}^2}{8\pi} \sim \left(\frac{B_{Gout}^2}{8\pi} + 2p_{out}\right) \quad (27)$$

Hereafter, we dropped the σ -related terms since $[(1 + \sigma_{in})/\sigma_{in}] \sim 1$. The guide field cases are more fluxed dominated than the anti-parallel case due to the guide field magnetic energy (Table 1). The effect of in-plane electric fields are included in the Poyting flux terms, as guide field contributions. In addition, flux conservation of the out-of-plane field yields

$$B_{Gin}L_{in}v_{in} = B_{Gout}L_{out}v_{out} \quad (28)$$

Combining eqs. 12, 26, and 27, we obtain

$$\frac{L_{in}v_{in}}{L_{out}v_{out}} \sim \frac{8\gamma_{out}^2 p_{out} + (B_{out}^2 + B_{Gout}^2)/4\pi}{4p_{out} + (B_{Gout}^2)/4\pi} \quad (29)$$

This immediately tells

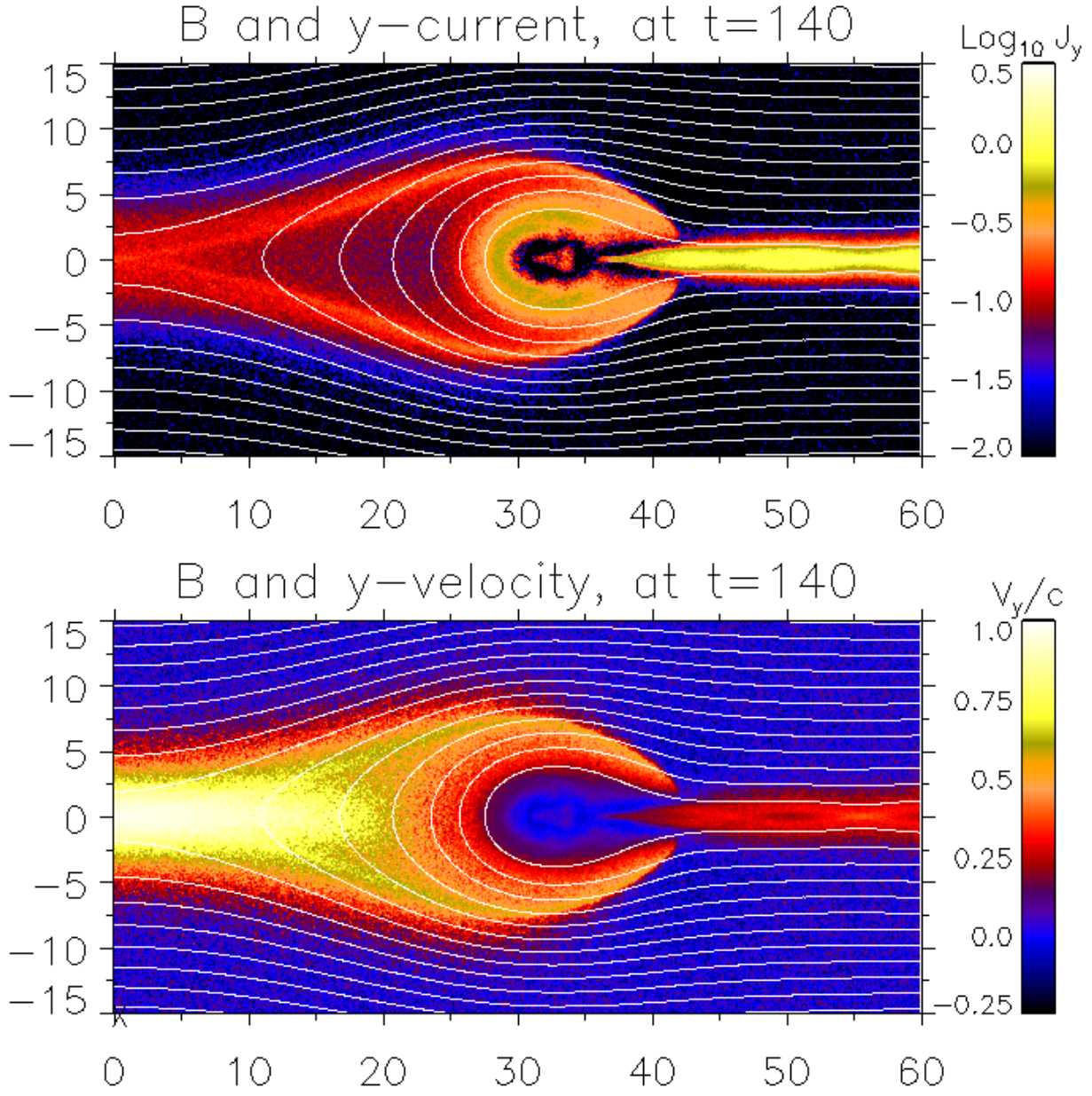
$$\frac{\gamma_{out}n_{out}}{\gamma_{in}n_{in}} \sim \frac{L_{in}v_{in}}{L_{out}v_{out}} \gtrsim 1 \quad (30)$$

and then eq. 28 yields

$$B_{Gin} \lesssim B_{Gout} \quad (31)$$

So, the guide field is compressed in the outflow region. For guide field larger than the anti-parallel component $B_{in} \lesssim B_{Gin}$, more energy is stored in B_{Gout} in the outflow region. As the guide field becomes even stronger, the guide field term becomes the largest contributor in eq. 29 and then eq. 30 becomes closer to the unity. This means that the guide field brings incompressibility in the simulation frame. In the strong guide field limit, we employ an incompressible condition

$$\gamma_{in}n_{in} \sim d_{cs} \sim \gamma_{out}n_{out} \quad (32)$$



▣

Fig. 5.— Magnetic field lines and y component of (a) the current density and (b) the average velocity at $t/\tau_c = 140$ in run 3.

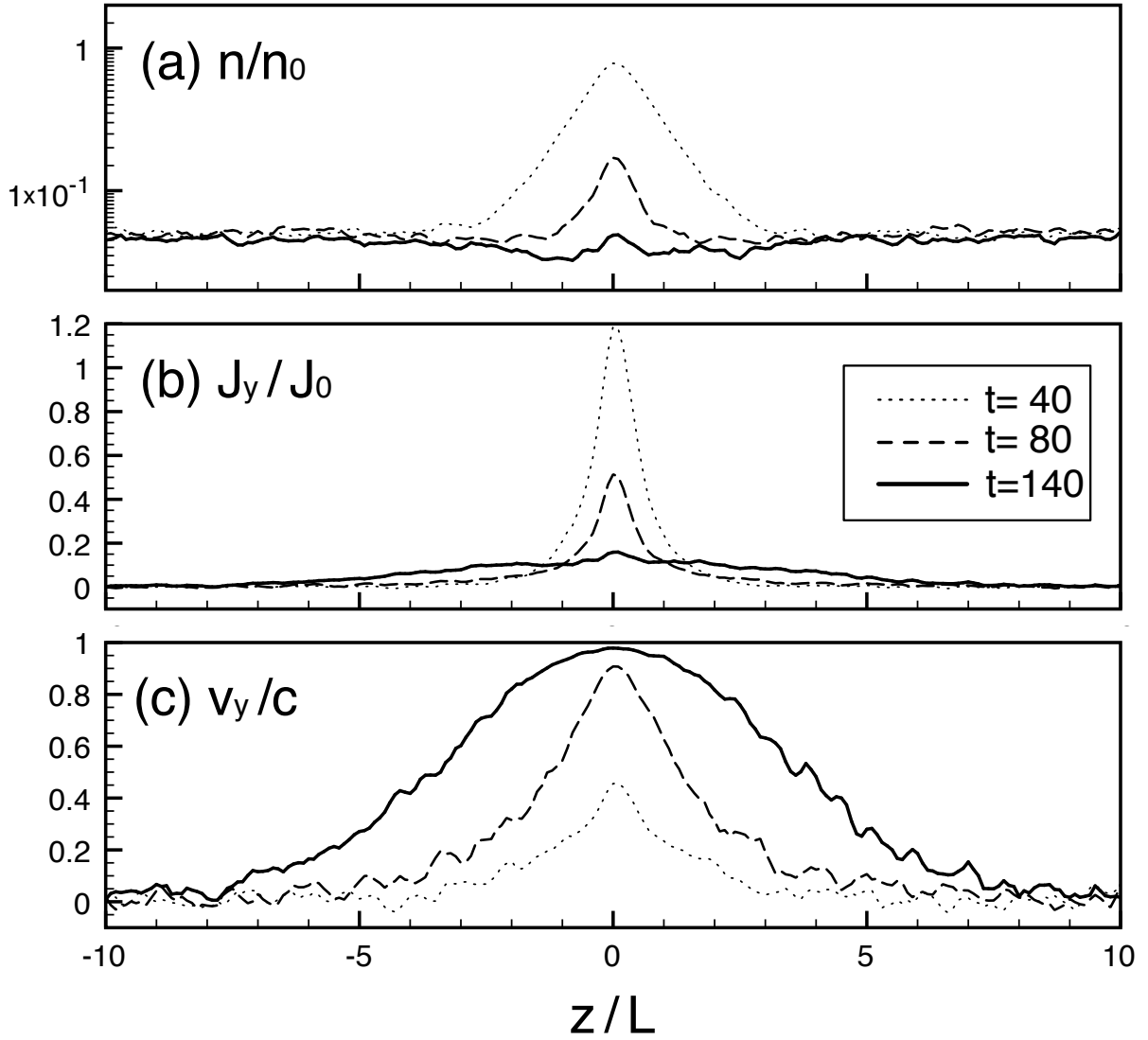


Fig. 6.— Physical properties along the inflow region at $x/L = 0$ (a) Normalized plasma density. (b) y -component of the electric current. (c) y -component of the plasma average velocity.

and then we obtain a condition similar to eq. 25 for the strong guide field limit

$$D_G = \frac{(\gamma_\beta n_0)}{n_{bg}} \beta \gtrsim 1, \quad (33)$$

where D_G is the discriminant term or the minimum relative thickness. It is significant that D_G only depends on the initial configuration parameters, while the antiparallel counterpart D (eq. 25) contains a variable γ_{out} , which comes from the plasma compressibility effect (eq. 22). As a result, the sufficient condition is more easily satisfied than in the anti-parallel case, so that the current sheet expansion is more significant.

The temporal evolutions of the current layer thickness in guide field runs are presented by the *dashed line* in Fig. 3a. In the guide field cases, time is re-arranged by some offsets ($\Delta t = 60\tau_c$) due to the late onset of reconnection, so that we can directly compare their thickness in the expanding phase. In the guide field cases, the current sheet originally becomes thinner during the long pre-onset stage of reconnection. In the case of run 3, the outflow guide field is $B_{Gout} \sim 1.7B_0$ and so the system seems to be sufficiently incompressible. The sufficient condition (eq. 33) yields $D_G = 6 > 1$, which predicts that the current sheet expands up to a factor of 6 in the strong guide field limit. Considering the weak compressibility, this is well consistent with the observed thickness of $4\text{-}5L$ (Fig. 3). In the case of run 4, the current sheet expands slowly (*dotted line* in Fig. 3a), due to the slowest evolution of reconnection. The condition is $D_G = 1.5 > 1$ in the guide field limit, which is roughly consistent with the asymptotic thickness of the current sheet: $\sim 1.3L$. The parameter D_G may be a good approximation of the thickness in the guide field cases. One reason is that plasmas are nearly incompressible. The other reason is that the plasma y -velocity is closer to the light speed $\langle v_y \rangle \sim 0.9c$, because their motions are threaded by the guide field.

5. DISCUSSION & SUMMARY

We demonstrated that the relativistic reconnecting current sheet self-regulates its thickness, so that it facilitates the fast reconnection rate. In order to study the aspect ratio of the diffusion region, many attentions have been paid to the length of the diffusion region. However, it is found that relativistic reconnecting layer changes the aspect ratio by expanding its thickness, and that we obtain higher reconnection rate. Zenitani & Hoshino (2001) briefly reported the current sheet expansion and argued that the relativistic mass increases the meandering width. This explains some aspects, but the situation is more complicated. Indeed, due to the enhanced reconnection electric field E_y , some incoming plasmas start (relativistic) meandering motion around the neutral plane ($z = 0$), while others are directly driven

to the $\pm y$ directions without reaching the neutral plane. The current sheet expansion arises from the net effect that contains all particle motions there. Bessho & Bhattacharjee (2007) reported the faster reconnection rate in lower-dense background condition. That trend can be consistently explained by our theory. Based on a relativistic Sweet-Parker analysis, we developed physical interpretations and derived some critical conditions. It is found that the current sheet is likely to expand when the reconnection inflow is flux dominated, and it further expands when the guide field is strong. Although the guide field effect is unclear in the dense background runs (runs 2 and 4), low-dense cases exhibited a significant difference (runs 1 and 3). In other words, high- σ (low-dense) limit of astrophysical interests, the guide field may play a crucial role in the reconnection topology by expanding the current sheet.

We also found that the relativistic Sweet-Parker model should be treated compressibly. In fact, our simulation snapshot shows the density ratio of $\gtrsim 2$ in the steady state (e.g. Fig. 2a). Previous authors (Blackman & Field 1994; Lyutikov & Uzdensky 2003) assumed plasma incompressibility, but these models should be re-constructed under the compressible condition, especially when the outflow Lorentz factor can be large ($\gamma_{out} \gg 1$), unless the guide field is strong enough. The relativistic Petschek models (Blackman & Field 1994; Lyubarsky 2005; Tolstykh et al. 2007) are out of scope of the present study, but our analysis on the guide field reconnection supports Lyubarsky (2005)’s argument that the guide field changes the dynamics of reconnection. In our case, the guide field introduces the incompressibility, and then the current sheet is more likely to self-regulate.

We find another new result regarding the outflow speed. In the non-relativistic regime, the reconnection outflow speed is often approximated by the inflow Alfvén speed. If this can be applied to the relativistic cases $\gamma_{out}^2 \sim \gamma_{Ain}^2 \sim (1 + \sigma_{in}) \sim \sigma_{in}$, eq. 8 implies that the critical condition (eq. 25) is insensitive to $(\gamma_{\beta} n_0)/n_{bg}$ or σ_{in} . However, in our simulations, the obtained outflow Lorentz factor γ_{out} is substantially slower than that of inflow Alfvén speed (γ_{Ain}). The outflow velocity is insensitive or weakly sensitive to the inflow flux σ_{in} , and therefore, the current sheet expansion does depend on $(\gamma_{\beta} n_0)/n_{bg}$. It is reasonable that the current sheet expansion is more significant when reconnection inflow is more flux dominated, because it contains less current carriers. There are several reasons why reconnection outflow is “slow”. One reason is that reconnection is unsteady. The reconnection jet slows down because it pushes away the pre-existing plasmas at the outflow region in unsteady simulations. This will be checked by the PIC simulations with open boundary conditions. Another is the relativistic pressure effect. In the relativistic regime, a relativistically high pressure increases the plasma enthalpy (eq. 12), which works as an effective inertia, and then bulk speed becomes slower. In order to maintain the current sheet against the strong magnetic pressure (eq. 13), a relativistically high pressure is required. We can see this from a calculation, which neglects pressure effects. Without the pressure terms, the energy and

number conservation (eqs. 4 and 5) read

$$(1 + \sigma_{in})2\gamma_{in}^2 w_{in} L_{in} v_{in} \sim 2\gamma_{out}^2 w_{out} L_{out} v_{out} \quad (34)$$

$$\frac{2\gamma_{out}^2 w_{out}}{2\gamma_{in}^2 w_{in}} \sim \frac{\gamma_{out}^2 n_{out}}{\gamma_{in}^2 n_{in}} = \frac{\gamma_{out}}{\gamma_{in}} \frac{L_{in} v_{in}}{L_{out} v_{out}} \quad (35)$$

From the equations, we would obtain an unrealistic super-Alfvénic outflow: $\gamma_{out} \sim (1 + \sigma_{in})\gamma_{in} \gg \gamma_{Ain}$ (Lyutikov & Uzdensky 2003). As a result, we conclude that the pressure effect is critical.

Compared with one fluid approximation, our model deals with both electron fluid and positron fluid independently. Therefore, the number/energy budget conditions are more reliable, and we can also discuss the y -velocity $|v_y| < c$. Instead, the difficulty is that several parameters (d_{cs} , γ_{out} , v_{out} and v_y) still have freedom in the current sheet or in the outflow region. The electron/positron fluids with high Lorentz factor γ_{out} may flow toward the x direction or toward the $\pm y$ directions. The reasonable criteria $(v_y^2 + v_{out}^2) < c^2$ in the outflow region will improve the model.

It is reasonable that the conditions (eqs. 25 and 33) are reciprocal to the drift speed parameter β . When the initial drift speed is fast, the current sheet is relatively thin, so that it is more likely to expand. However, in the relativistic speed limit of $\beta \rightarrow 1$, the current sheet is likely to expand before the large-scale reconnection evolves due to the various instabilities (e.g. the tearing instability or the drift kink instability). In the vacuum inflow limit of $n_{bg} \rightarrow 0$, eventually magnetic reconnection will disappear because there is no plasmas to carry the steady current. The induced electric field simply travels away as an electromagnetic wave, without accelerating plasmas. We do not know whether the transition is smooth or drastic, from the self-regulated current sheet to the quiet vacuum condition. The self-regulation of the current sheet will be found in relativistic reconnection in an ion-electron plasma, too. When the electron drift speed increases to an order of c , the electron current layer will similarly expand, while it is unclear that the enhanced electric field accelerates ions. When the broadened electron layer becomes comparable to the ion layer, ions and electrons more effectively interact each other, and then it may affect the reconnection structure once again.

In summary, we demonstrated that the relativistic reconnecting current sheet self-regulates its thickness, in order to carry the required current. A simple Sweet-Parker analysis shows that the current sheet expansion is dominant in the flux-dominated inflow, and that the guide field enhances the current sheet expansion. It is also noteworthy that the relativistic Sweet-Parker reconnection is compressible, and that it is incompressible only in the limit of the strong guide field.

The authors are grateful to A. Klimas, M. Kuznetsova and H. Takahashi for useful

Table 1: List of Simulation runs

Run	1	2	3	4
T/mc^2	1	1	1	1
B_G/B_0	0	0	1.5	1.5
$n_{bg}/\gamma_\beta n_0$	0.05	0.2	0.05	0.2
σ_{in}	~ 36	~ 9	~ 115	~ 30
v_{out}/c	~ 0.7	~ 0.4	~ 0.3	~ 0.3
γ_{out}^2	~ 2	~ 1.3	$\sim 3-4$	~ 1.2

discussions. The authors also thanks the anonymous referee for his/her constructive comments and careful evaluation of this manuscript. This research was supported by facilitates of JAXA/ISAS, the NASA Center for Computational Sciences, and NASA’s MMS SMART mission. One of the authors (S. Z.) gratefully acknowledges support from NASA’s postdoctoral program.

REFERENCES

- N. Bessho and A. Bhattacharjee 2007, *Phys. Plasmas* , 14, 056503
- E. G. Blackman and G. B. Field 1994, *Phys. Rev. Lett.* , 72, 494
- J. Birn and E. R. Priest 2007, “Reconnection of Magnetic Fields: Magnetohydrodynamics and Collisionless Theory and Observations”, Cambridge University Press
- D. Biskamp 2000, “Magnetic Reconnection in Plasmas”, Cambridge University Press
- F. V. Coroniti 1990, *Astrophys. J.* , 349, 538
- W. Daughton, J. Scudder and H. Karimabadi 2006, *Phys. Plasmas* , 13, 2101
- G. Drenkhahn and H. C. Spruit 2002, *Astron. Astrophys.* , 391, 1141
- K. Fujimoto 2006, *Phys. Plasmas* , 13, 2904
- M. Hesse and D. Winske 1994, *J. Geophys. Res.* , 103, 26479
- M. Hesse, K. Schindler, J. Birn and M. Kuznetsova 1999, *Phys. Plasmas* , 6, 1781
- M. Hesse, M. Kuznetsova and J. Birn 2004, *Phys. Plasmas* , 11, 5387
- M. Hesse and S. Zenitani 2007, *Phys. Plasmas* , 14, 112102

- R. Horiuchi and T. Sato 1994, *Phys. Plasmas* , 1, 3587
- C. H. Jaroschek, R. A. Treumann, H. Lesch and M. Scholer 2004, *Phys. Plasmas* , 11, 1151
- M. Karlický 2008, *Astrophys. J.* , 674, 1211
- Y. Lyubarsky 2005, *Monthly Notices of the RAS* , 358, 113
- M. Lyutikov 2003, *Monthly Notices of the RAS* , 346, 540
- M. Lyutikov and D. Uzdensky 2003, *Astrophys. J.* , 589, 893
- M. A. Shay, J. F. Drake and M. Swisdak 2007, *Phys. Rev. Lett.* , 99, 155002
- Y. V. Tolstykh, V. S. Semenov, H. K. Biernat, M. F. Heyn and T. Penz 2007, *Advances in Space Research*, 40, 1538
- V. M. Vasyliunas 1975, *Reviews of Geophysics and Space Physics*, 13, 303
- N. Watanabe and T. Yokoyama 2006, *Astrophys. J.* , 647, L123
- S. Zenitani and M. Hoshino 2001, *Astrophys. J.* , 562, L63
- S. Zenitani and M. Hoshino 2005b, *Phys. Rev. Lett.* , 95, 095001
- S. Zenitani and M. Hoshino 2007, *Astrophys. J.* , 670, 702
- S. Zenitani and M. Hoshino 2008, *Astrophys. J.* , 677, 530